Eclética Química

Original article

revista.iq.unesp.br

| Vol. 48 | n. 3 | 2023 |

Novel organophosphorus Schiff base ligands: Synthesis, characterization, ligational aspects, XRD and biological activity studies

Yasmin Mos'ad Jamil[1+], Fathi Mohammed Al-Azab[1], Nedhal Abdulmawla Al-Selwi[1]

1. Sana'a University, Faculty of Science, Sana'a, Yemen.

+Corresponding author: Yasmin Mos'ad Jamil, **Phone:** +967 771952842, **Email address:** y.jamil@su.edu.ye

ARTICLE INFO

Article history:
Received: November 03, 2022
Accepted: May 05, 2023
Published: July 01, 2023

Section Editors: Assis Vicente Benedetti

Keywords:
1. antimicrobial activity
2. antioxidant activity
3. nanoparticles
4. X-ray diffraction

ABSTRACT: Six complexes have been synthesized from Cu(II), Ni(II), and Co(II) with new bidentate N_2 donor Schiff base ligand (2-methoxybenzalidene-1-phenylsemicarbazide **L_1**) and tridentate N_2O donor organophosphorus Schiff base ligand (2-methoxybenzalidenediphenylphosphate-1-phenylsemicarbazide **L_2**). Both ligands were synthesized and characterized by metal analysis, infrared (IR), ultraviolet visible (UV-Vis), and nuclear magnetic resonance (NMR) spectral studies. The chemical structures of the synthesized complexes were characterized using their metal analysis, magnetic susceptibility, molar conductance, IR, and UV-Vis spectra. According to molar ratio studies, the complexes have the composition of ML_2 for **L_1** and ML for **L_2**. The X-ray diffraction (XRD) studies showed that the particle size of ligands and **L_1** complexes were in nano-range. The ligands and their metal complexes have been screened for their antioxidant, antibacterial and antifungal activity.

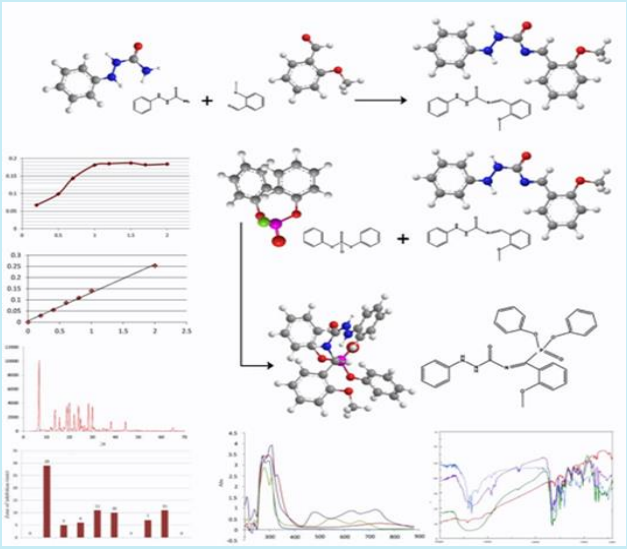

ISSN: 1678-4618
DOI: 10.26850/1678-4618eqj.v48.3.2023.p36-53

1. Introduction

Schiff base compounds are commonly used as ligands in inorganic chemistry to create stable complexes with different transition metal ions (Abu-Dief *et al*., 2021). They are prepared by a condensation reaction of aromatic/aliphatic aldehydes and amines to form an azomethine group (CH=N) (Abu-Yamin *et al*., 2022). In previous research, many biological activities of Schiff base compounds have been documented including antibacterial, antifungal, antimalarial, antiproliferative, analgesic, anti-inflammatory, antiviral, antipyretic, and anticancer properties (Camellia *et al*., 2022; Ceramella *et al.*, 2022; Ibeji *et al*., 2022; Jamil *et al*., 2023; Kaczmarek *et al*., 2018; Kafi-Ahmadi and Marjani, 2019; Song *et al*., 2020). A survey of the literature reveals a work devoted to the synthesis, characterization, and biological activities of many metal complexes of Schiff base from 2-methoxybenzaldyde (Camellia *et al*., 2022; Ibeji *et al*., 2022; Sani and Iliyasu, 2018; Yusof *et al*., 2015) In addition, organophosphorus compounds with transition metal ions have been the subject of several studies since complexes of such compounds exhibit biological activity (Abd El-Wahab and El-Sarrag, 2004; Brzezińska-Błaszczyk *et al*., 1996; El-khazandar, 1997; Ochocki *et al*., 1995). Hence, in the present study, a new Schiff base of 2-methoxybenzaldyde and 1-phenylsemicarbazide, its organophosphorus Schiff base, and their complexes with Cu^{2+}, Ni^{2+}, and Co^{2+} were prepared and characterized. The biological activities were investigated for these compounds, such as their antibacterial and antioxidant.

2. Experimental

2.1 Materials

The chemicals, 1-phenylsemicarbazide (Riedel-de Haën), 2-methoxybenzaldyde (Aldrich), diphenyl chlorophosphate (Riedel-de Haën), Triethyl amine (Riedel-de Haën), bipyridine (Aldrich), ferric chloride (Aldrich), ascorbic acid (BDH), sodium acetate trihydrate (BDH), glacial acetic acid (BDH) and metals chloride hydrate ($CuCl_2.2H_2O$, $NiCl_2.6H_2O$, and $CoCl_2.6H_2O$) were purchased from BDH. The solvents used were of spectroscopic grade.

2.2 Physical measurements

Elemental analysis for C, H, and N was performed with a Vario EL Fab. CHN Nr, at Central Laboratory, Faculty of Science, Cairo University, Giza, Egypt. Conductivity measurements were done with a Jenway conductivity meter model 4510 in dimethylformamide (DMF). The magnetic moments were determined by Gouy's method using a magnetic susceptibility balance from Johnson Metthey and Sherwood model. Ultraviolet visible (UV-vis) spectra were measured with (Specord200, Analytilk Jena, Germany) in the range of 200–900 nm, at Sana'a University. Fourier-transform infrared (FT-IR) spectra were recorded in transmission mode by an (FT/IR-140, Jasco, Japan) spectrophotometer in the wavenumber range of 4000–400 cm^{-1} (KBr was used as a matrix material for pellets). ^1H and ^{13}C NMR spectra for ligands were performed in d_6-DMSO solvent using tetramethylsilane as an internal standard, at Cairo University, Giza, Egypt. All melting points reported for the compounds are measured in glass capillary tubes in Celsius degrees. Chloride was determined gravimetrically by silver nitrate (Vogel, 1961). The amount of coordinated and uncoordinated water molecules was determined gravimetrically using the weight loss method (Vogel, 1961). The X-ray diffraction (XRD) patterns were obtained using XD-2 (Shimadzu ED-720) powder X-ray diffractometer at a voltage of 35 kV and a current of 20 mA using CuK(α) radiation in the range of $5° < 2\theta < 70°$ at 1° min^{-1} scanning rate and a wavelength 1.54056 Å at Yemen Geological Survey and Mineral Resources Board.

2.3 Synthesis of ligands

2.3.1 Synthesis of Schiff base (2-methoxybenzalidene-1-phenylsemicarbazide ***L₁****)*

The reaction mixture, including an ethanolic solution of amine (1-phenylsemicarbazide) (7.55 g, 0.05 mol) with an ethanolic solution of aldehyde (2-methoxybenzaldyde) (6.80 g, 0.05 mol) was refluxed on hot reflux under constant stirring for 2–3 h, then the product was separated on cooling, it was filtered, washed several times with ethanol and ether, then the obtained crystals product was recrystallized by ethanol to give the corresponding Schiff base. The reaction is given in Fig. 1.

Eclética Química, vol. 48, n. 3, 2023, 36-53
ISSN: 1678-4618
DOI: 10.26850/1678-4618eqj.v48.3.2023.p36-53

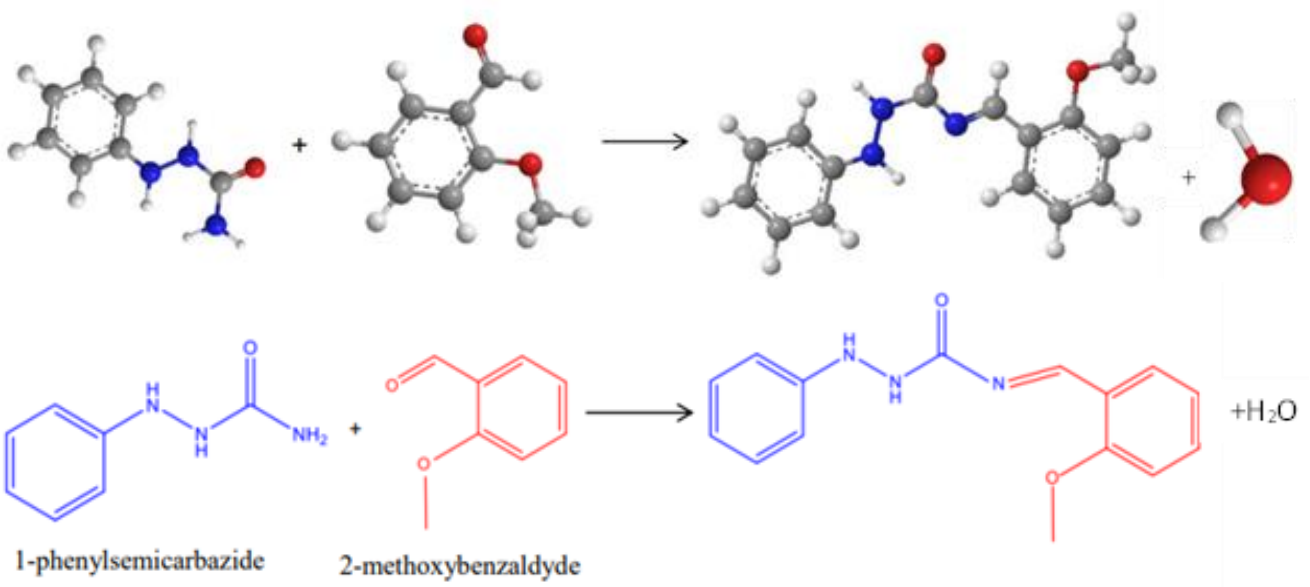

Figure 1. Preparation of Schiff base 2-methoxybenzalidene-1-phenylsemicarbazide $\mathbf{L_1}$.

2.3.2 Synthesis of organophosphorus Schiff base (2-methoxybenzalidenediphenylphosphate-1-phenylsemicarbazide $\mathbf{L_2}$)

The organophosphorus Schiff base $\mathbf{L_2}$ was prepared by condensation between a solution of Schiff base (4.03 g, 0.015 mol) in dry benzene (50 mL) with a solution of diphenyl chlorophosphate (3.69 g, 0.015 mol) in dry benzene (50 mL) in 1:1 molar ratio in presence of triethyl amine (Fig. 2). After complete addition, the reaction mixture was heated under reflux for 2 h. The formed solid (triethyl amine hydrochloride) was filtered and the product was obtained after evaporation in a water bath.

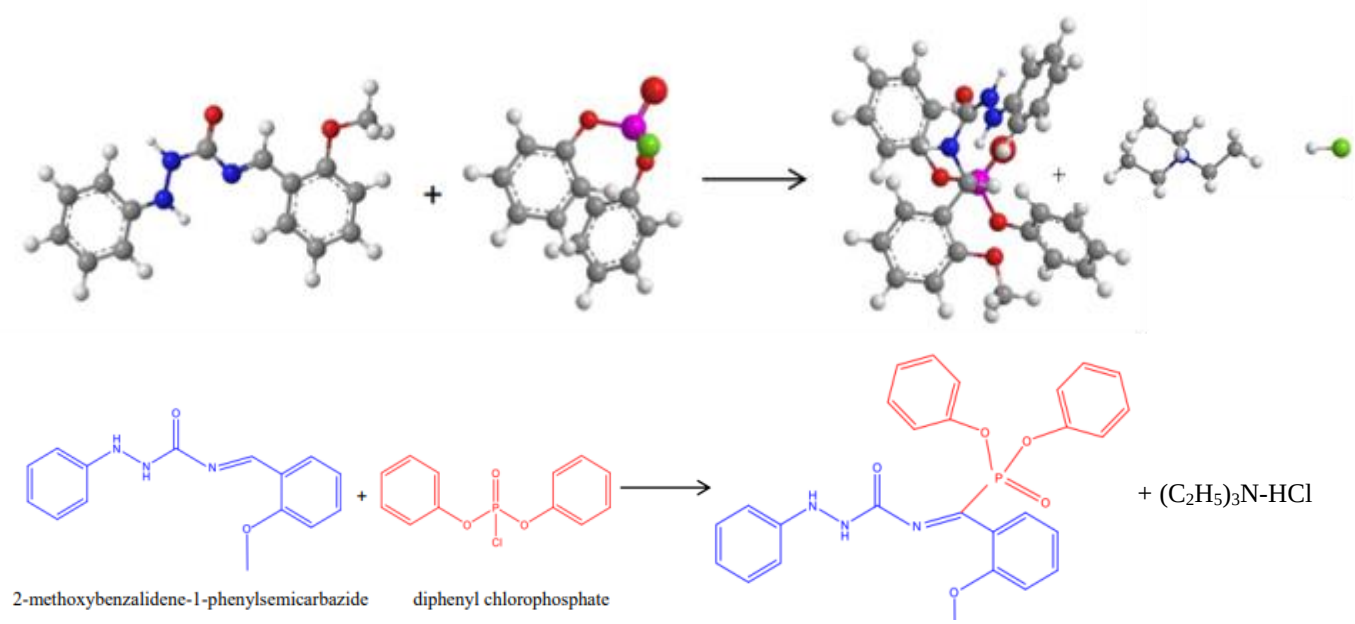

Figure 2. Preparation of organophosphorus Schiff base 2-methoxybenzalidenediphenylphosphate-1-phenylsemicarbazide $\mathbf{L_2}$.

Eclética Química, vol. 48, n. 3, 2023, 36-53
ISSN: 1678-4618
DOI: 10.26850/1678-4618eqj.v48.3.2023.p36-53

2.4 Synthesis of metal complexes

2.4.1 Synthesis of Schiff base metal complexes

A hot ethanolic solution of metal chloride was added dropwise to an ethanolic solution of Schiff base (2 L:1 mol L^{-1}) molar ratio. The mixture was refluxed on a hot plate with stirring for 2–3 h. After evaporation of the solvent, the solid product was washed several times with ethanol and dried over anhydrous $CaCl_2$.

2.4.2 Synthesis of organophosphorus Schiff base metal complexes

A solution of metal chloride in 20 mL absolute ethanol was added dropwise to the solution of organophosphorus Schiff base in warm absolute ethanol (1 L: 1 mol L^{-1}). After the addition, the mixture was heated under hot reflux for three hours. The solution was evaporated, and the solid complexes were collected using ether.

2.5 Determination of the stoichiometry of the formed complexes of molecular structure (Molar ratio method)

The molar ratio method was described by the Molar ratio method (Yoe and Jones, 1944). The concentrations of metal ions (Cu^{2+}, Ni^{2+}, and Co^{2+}) were kept constant at (1×10^{-3} mol L^{-1}) in methanol and the concentration of ligands (**L_1** and **L_2**) was regularly varied in methanol. The absorbance of the prepared solutions was measured at the constant wavelength (λ_{max}). The absorbance values were plotted versus the molar ratio [ligand] / [metal ion]. The intersections of the obtained straight lines indicate the molar ratio of the stable complexes.

2.6 Crystallinity and particle size from XRD

The percentage of crystallinity, XC (%) was calculated based on the integrated peak areas of the principal peaks (Shah *et al*., 2006). The crystallinity of the complexes is calculated relative to the crystallinity of the ligands as a ratio (Eq. 1):

$$X_C\ (\%) = \frac{A_{complex}}{A_{ligand}} \times 100 \qquad (1)$$

where $\boldsymbol{A_{complex}}$ and $\boldsymbol{A_{ligand}}$ are the areas under the principal peaks of the complex and ligand sample, respectively.

X-ray diffraction was also used to determine the average particle size (D) which was estimated by the Scherrer equation (Akhtar *et al*., 2015; Patterson, 1939) (Eq. 2):

$$D = \frac{K\,\lambda}{\beta\,cos\theta} \qquad (2)$$

where $\boldsymbol{K}$ is Scherrer constant and equals 0.94, $\boldsymbol{\lambda}$ is the X-ray wavelength of Cu-Kα radiations (1.5405 Å), $\boldsymbol{\beta}$ is full width at half maximum (FWHM) and $\boldsymbol{\theta}$ is Bragg diffraction angle in degrees.

2.7 Antioxidant activity

The total antioxidant activity of the compounds has been studied using ferric-bipyridine reducing capacity (FBRC) (Al-Azab *et al*., 2023). It was taken (1 mL, 10^{-2} mol L^{-1} $FeCl_3.6H_2O$) to 10 mL volumetric flask different volumes of the standard antioxidant ascorbic acid (0.1 g L^{-1}) were added (0.01, 0.02, 0.04, 0.06, 0.08, 0.1, 0.2 mL). This was followed by 2.0 mL 0.3 mol L^{-1} acetate buffer (pH 4) and 1.0 mL bipyridine (6.4×10^{-3} mol L^{-1}). The volume was completed to the mark with deionized water. After 10 min of incubation at room temperature, the absorbance was recorded against a blank at 535 nm. The absorbance values were plotted against the concentration of the various antioxidant solutions (Fig. 3). Similarly, 0.02 mL of (0.1 mg mL^{-1} methanol) of each tested compound was reacted with 1 mL, 10^{-2} mol L^{-1} $FeCl_3.6H_2O$ solution, (6.4×10^{-3} mol L^{-1}) bipyridine and 2.0 mL 0.3 mol L^{-1} acetate buffer (pH 4). This mixture was diluted to 10 mL with deionized water for the antioxidant assay. The fixed reaction time and fixed state measurement method were used to find out the antioxidant activity of these compounds in methanol as a solvent. All spectrophotometric measurements were measured using UV-vis spectrophotometer (Specord200, Analytikjena, Germany) at Sana'a University.

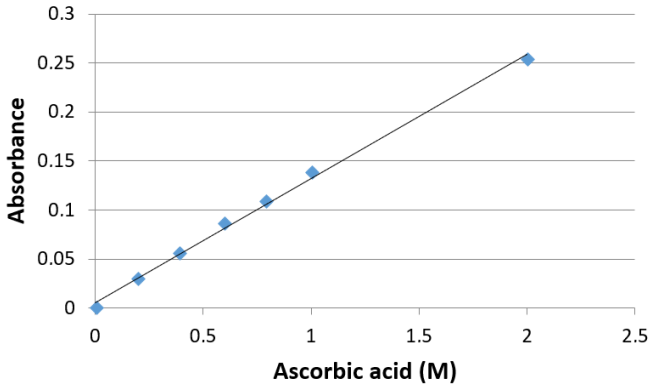

Figure 3. Calibration curve of ascorbic acid with Fe-Bp complex.

Eclética Química, vol. 48, n. 3, 2023, 36-53
ISSN: 1678-4618
DOI: 10.26850/1678-4618eqj.v48.3.2023.p36-53

2.8 Antimicrobial activity

The synthesis compounds were exanimated for their antimicrobial activity in the Laboratory of Microbiology at Sana'a University. They Germinated four types of bacteria (*Staphylococcus aureus*, *Bacillus subtilis*, *Escherichia coli*, and *Pseudomonas aeruginosa*) and one fungus (*Candida albicans*) on nutrient agar and Sabouraud agar solid media respectively. Using the filter paper disc method (Ericsson *et al*., 1960), it was prepared one concentration from each compound (1000 µg mL^{-1}) in DMSO. Then added (100 µL) from each prepared compound on a filter paper (Whatman No. l filter paper, 5 mm diameter) which contained the bacteria with agar solid media, all the Petri dishes were put in an incubation period at 37 °C for 24 h. Gentamicin 120 µg mL^{-1} was used as a reference substance for bacteria and Mycostatin 30 µg mL^{-1} for fungi. The results were registered by calculating the diameter of the inhibition zone (mm).

3. Results and discussion

The Schiff base ligand (**L_1**) was prepared by the condensation of 1-phenylsemicarbazide with 2-methoxybenzaldyde in the molar ratio 1:1. The organophosphorus ligand (**L_2**) was prepared by the condensation of diphenylchlorophosphate with the prepared Schiff base (**L_1**) in the molar ratio 1:1. The ligand ratio of (**L_1**) with Cu(II), Ni(II), and Co(II) complexes was found to be 1:2, and the ligand ratio of (**L_2**) with Cu(II), Ni(II), and Co(II) complexes were found to be 1:1. The molar conductance data of the complexes of **L_1** are 18.44, 20.31, and 21.09 Ω^{-1} cm^2 mol^{-1} in DMF (1×10^{-3} mol L^{-1}). These results show that these complexes are non-electrolytes (Aderoju and Sherifah, 2015; Geary, 1971), so the complexes of **L_1** are insoluble in water and common organic solvents but soluble in polar solvents such as DMF and DMSO. The non-electrolytic nature of these complexes suggests that the chloride anions of the three salts have coordinated with the **L_1** chelate of metal complexes. The reaction of the synthesized **L_1** complexes with silver nitrate have been not given a white precipitate, and after digestion with nitric acid, the silver nitrate test gave a positive result. Furthermore, the results of molar conductance of **L_2** complexes (73.75, 84.93, and 77.79) show that these complexes are 1:1 electrolytes in DMF (1×10^{-3} mol L^{-1}) (Geary, 1971; Shakdofa *et al*., 2017). The complexes of **L_2** are slightly soluble in water and soluble in common organic solvents. In the case of **L_2** complexes, the precipitation was observed upon the addition of silver nitrate to the solution of the complexes (Vogel, 1961).

L_1 and **L_2** and their complexes were characterized by elemental analyses, FT-IR, ^{1}HNMR, and electronic spectra which are compliant with the proposed structures as shown in Fig. 4a and b. Table 1 lists some physical and analytical data on the ligands and their complexes.

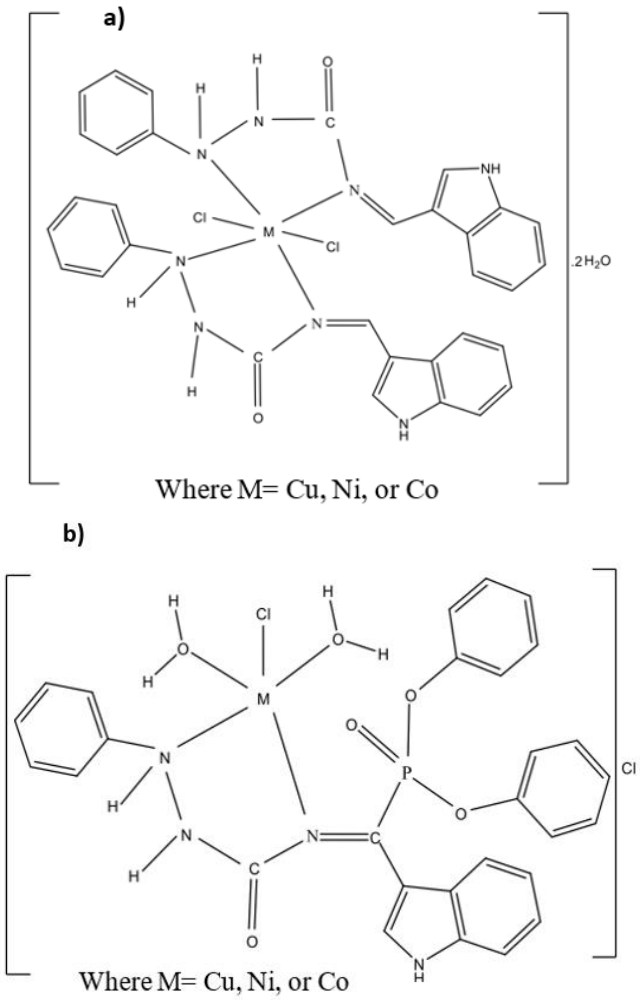

Figure 4. Proposed structure of **(a) L_1** complexes; **(b) L_2** complexes.

Eclética Química, vol. 48, n. 3, 2023, 36-53
ISSN: 1678-4618
DOI: 10.26850/1678-4618eqj.v48.3.2023.p36-53

Table 1. Some physical properties and elemental analysis of the ligands and their complexes.

Compound	Color (Yield)	M.P. (°C)	Λm (Ω^{-1} cm^2 mol^{-1})	F.Wt (g mol^{-1})	Elemental analysis calculated% (found)				
					C	H	N	P	M
$C_{12}H_{11}N_3O_2$(L_1)	White (70%)	174	-	269.30	66.90 (67.04)	5.61 (5.78)	15.60 (15.27)	-	-
$C_{23}H_{10}N_3O_5P$(L_2)	Brown (75%)	153	-	479.36	65.15 (64.96)	2.94 (3.19)	8.76 (8.90)	7.05 (6.89)	-
[Cu(L_1)$_2$Cl$_2$]·2H$_2$O	Green (70%)	240	18.44	709.08	50.81 (51.30)	4.83 (4.88)	11.85 (12.08)	-	8.96 (9.00)
[Ni(L_1)$_2$Cl$_2$]·2H$_2$O	Green (50%)	250	20.31	704.22	51.16 (50.99)	4.87 (5.02)	11.93 (12.20)	-	8.33 (8.75)
[Co(L_1)$_2$Cl$_2$]·2H$_2$O	Dark blue (57%)	220	21.09	704.46	51.14 (51.36)	4.86 (4.33)	11.92 (11.68)	-	8.36 (8.13)
[Cu(L_2)Cl (H$_2$O)$_2$].Cl	Dark red (17%)	130	73.75	649.84	48.05 (47.85)	2.79 (2.86)	12.93 (13.18)	4.76 (4.55)	9.77 (9.53)
[Ni(L_2)Cl (H$_2$O)$_2$].Cl	Red (19%)	108	84.93	644.98	48.41 (48.47)	2.82 (3.00)	13.02 (12.79)	4.80 (4.70)	9.09 (9.00)
[Co(L_2)Cl (H$_2$O)$_2$].Cl	Red (23%)	112	77.79	645.22	48.39 (48.01)	2.81 (2.57)	13.02 (13.24)	4.79 (4.99)	9.13 (8.98)

3.1 Nuclear magnetic resonance spectral studies

3.1.1 ^{1}HNMR spectra of the ligands

The ^{1}HNMR spectra of the ligands **L₁** and **L₂** (Figs. S1 and S2 see Supplementary Material) exhibited signals which are consistent with the proposed structure. The peaks at 6.019, 6.713, and 5.997, 6.692 ppm are assignable to the protons of the NH groups in the ligands **L₁** and **L₂** respectively (El-Tabl *et al.*, 2007; Shakdofa *et al.*, 2017). Azomethine proton appeared as a singlet signal at 8.656 ppm (s, 1H) in **L₁** (Çakır *et al.*, 2003) and this signal disappeared in the **L₂** spectrum due to a replacement reaction on this group with eliminated HCl and forming a P-C bond. The signals at 3.908 and 3.050 were assigned to (s, 3H, OCH_3) **L₁** and **L₂**, respectively (Çakır *et al.*, 2003). The peaks appearing in the range 6.742–7.831 and 6.717–7.842 ppm may correspond to protons of the aromatic hydrogen of **L₁** and **L₂** respectively (Galil *et al.*, 2015).

3.1.2 ^{13}CNMR Spectra of the ligands

The ^{13}CNMR spectra (Figs. S3 and S4 see Supplementary Material) showed singlet signals at 161.688 and 160.421 ppm that attributed to carbonyl carbon C=O of the ligands **L₁** and **L₂** respectively (Carrasco *et al.*, 2020; Galil *et al.*, 2015). Also, the spectra exhibited two peaks at δ 149.517 and δ 149.623 ppm that were able to be appointed to azomethine carbon C=N of the ligands **L₁** and **L₂**, respectively (Shakdofa *et al.*, 2017). The peaks between 111.241–130.917 and 112.189–130.143 ppm is attributed to aromatic carbon in **L₁** and **L₂**, respectively (Galil *et al.*, 2015). The carbon of the methoxy group appeared at 55.534 and 45.381 ppm in ligands **L₁** and **L₂**, respectively (Yusof *et al.*, 2015).

3.2 IR spectra of the ligands and their complexes

Important IR bands of the ligands and their complexes are given in Table 2 and Fig. 5a. The presence of IR bands at 1,655 and 1,602 cm^{-1} of ligand **L₁** assigned to υ(C=O) and υ(C=N) respectively (Hossain *et al.*, 2019). The strong bands at 3,334 and 3,397 cm^{-1} are assignable and attributed to υ(NH) of this ligand (Nakamoto, 1998). The bands showed at 3,057, 2,958, and 1,267 cm^{-1} belong to aromatic υ(C-H), aliphatic υ(C-H), and υ(-C-N) stretching mode of vibrations, respectively (Jassem *et al.*, 2013). The band at 2,853 cm^{-1} in its spectrum can be appointed to υ(-O-CH_3) (Mohapatra *et al.*, 2011).

The IR spectra of the complexes (Fig. 5a) are characterized by the appearance of broad bands at 3,424, 3,346, and 3,324 cm^{-1} due to the water molecules in L_1(Cu), L_1(Ni), and L_1(Co) complexes, respectively (González-García *et al.*, 2016). In the spectra of all the complexes, no change in the frequency of (C=O) but the 1,602 cm^{-1} band was shifted to a lower frequency indicating the involvement of the N atom of the azomethine group in coordination (Table 2). The bands of υ(NH, NH) disappeared in complexes due to the broad bands of water. New vibrations at 400–600 cm^{-1} that are not present in the free ligand are attributed to the existence of υ(M-N) and υ(M-NH) (Yassin *et al.*, 2020). Based on the observations, it has been suggested that the ligand **L₁** acts as bidentate.

Although the presence evidence of υ(M-Cl) could not be brought in the IR data due to instrumental limitation, the insolubility of **L₁** complexes in water and their non-

Eclética Química, vol. 48, n. 3, 2023, 36-53
ISSN: 1678-4618
DOI: 10.26850/1678-4618eqj.v48.3.2023.p36-53

electrolytic nature evinced that $2Cl^-$ coordinated with metal in **L_1** complexes.

In the ligand **L_2** spectrum (Fig. 5b), the bands observed at 1,654 and 1,591 cm^{-1} corresponds to υ(C=O) and υ(C=N), respectively (Hossain *et al*., 2019). The presence of υ(P=O) and υ(P-O-C) is indicated by the appearance of bands at 1,188 and 1,072 cm^{-1}, respectively (El-khazandar, 1997).

The coordinated water molecules with metal ions in the complexes were proved by the bands 3,347, 3,407, and 3,312 (Aderoju and Sherifah, 2015). The IR spectra of the metal complexes of ligand **L_2** (Fig. 5b) proposed that this ligand tridentate with the phosphoryl-oxygen, amine-nitrogen, and azomethine-nitrogen due to the shift in the position of υ(P=O), υ(-NH) and υ(C=N) (Table 2).

Table 2. The main IR absorption bands of the ligands and their complexes.

Compound	υ(H_2O)	υ(NH, NH)	υ(-O-CH_3)	υ(C=N)	υ(C=O)	υ(P=O)	υ(P-O-C)	υ(M-N)	υ(M-NH)
$C_{16}H_{14}N_4O(L_1)$	-	3398 3335	2853	1602	1655	-	-	-	-
$C_{27}H_{13}N_4O_4P$ (L_2)	-	3450 3347	2878	1591	1654	1188	1072	-	-
$[Cu(L_1)_2Cl_2]\cdot 2H_2O$	3424	3424	2850	1580	1651	-	-	527	428
$[Ni(L_1)_2Cl_2]\cdot 2H_2O$	3346	3346	2849	1571	1649	-	-	558	414
$[Co(L_1)_2Cl_2]\cdot 2H_2O$	3324	3324	2855	1577	1653	-	-	574	424
$[Cu(L_2)Cl\ (H_2O)_2].Cl$	3421	3467 3452	2866	1560	1650	1165	1072	516	410
$[Ni(L_2)Cl\ (H_2O)_2].Cl$	3407	3407	2850	1617	1655	1160	1067	520	458
$[Co(L_2)Cl\ (H_2O)_2].Cl$	3312	3365 3312	2846	1603	1651	1161	1068	517	467

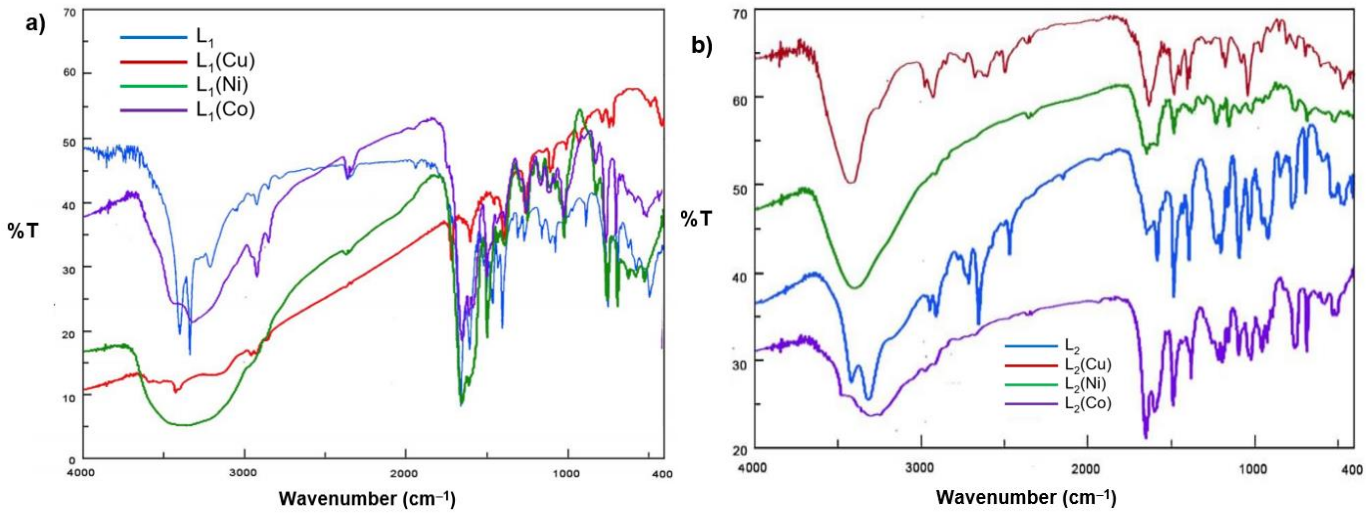

Figure 5. Infrared spectra. **(a) L_1** and its complexes; **(b) L_2** and its complexes.

3.3 Electronic spectra and magnetic measurements

The absorption spectra of the ligands **L_1** and **L_2** and their metal complexes were recorded in DMSO in the range of 200–900 nm (Table 3).

The ligands **L_1** and **L_2** exhibited two absorption bands (Figs. 6a and b) at 37,037.03, 35,714.28 and 33,333.33, 32,258.06 cm^{-1} that have been allocated for the π-π* and n-π* transitions, respectively (Mohammed *et al*., 2019). In the metal complexes, the transition of n-π* has been seen but they are shifted to another range. The shift in the transitions has been accounted for by the complexation between ligands with the metal ions.

The Cu complexes of **L_1** and **L_2** exhibited single broad absorption peaks at 13,513.51 and 13,333.33 cm^{-1} (Figs. 6a and b), respectively, attributable to the $^2Eg \rightarrow {}^2T_2g$ transition, indicating a distorted octahedral structure (Al-Maydama *et al*., 2008; Gup and Kirkan, 2005).

The electronic spectra of the **L_1**(Ni) and **L_2**(Ni) complexes (Figs. 5a and b) showed absorption bands at 18,181.81, 15,151.51 and 17,543.85, 15,151.51 cm^{-1}, respectively, attributable to the $^3A_2g \rightarrow {}^3T_1g(P)$ and $^3A_2g \rightarrow {}^3T_1g(F)$ transitions, which is compatible with this complex having the octahedral structure (Gup and Kirkan, 2005).

Eclética Química, vol. 48, n. 3, 2023, 36-53
ISSN: 1678-4618
DOI: 10.26850/1678-4618eqj.v48.3.2023.p36-53

The electronic spectra of the **L₁** and **L₂** complexes with Co (Figs. 6a and b) exhibited characteristic bands at 20,833.33, 15,873.01, 13,888.88 and 21,739.13, 20,000, 17,543.85 cm^{-1} assigned to $^4T_1g \rightarrow {}^4T_1g(P)$, $^4T_1g \rightarrow {}^4A_2g$ *and* $^4T_1g \rightarrow {}^4T_2g(F)$ transitions. These bands are associated with the octahedral structures (Gup and Kirkan, 2005).

This information with the effective magnetic moment (**μeff**) data (Table 3) of all complexes helped to support the suggested octahedral geometry (Al-Hakimi *et al.*, 2011; Fouda *et al.*, 2008).

Table 3. Electronic spectral and magnetic moment data of the ligands and their complexes.

Compound	μeff (B.M.)	(π→π*), transition	(n→π*) transition	d-d transition band (cm^{-1})	Assignments	Supposed structure
$C_{16}H_{14}N_4O(L_1)$	-	37,037.03	33,333.33	-	-	-
$C_{27}H_{13}N_4O_4P(L_2)$	-	35,714.28	32,258.06	-	-	-
$[Cu(L_1)_2Cl_2].2H_2O$	1.88	34,482.75	30,303.03	13,513.51	$^2Eg \rightarrow {}^2T_2g$	Distorted Octahedral
$[Ni(L_1)_2Cl_2]\cdot 2H_2O$	2.75	35,714.28	32,258.06	18,181.81 15,151.51	$^3A_2g \rightarrow {}^3T_1g(P)$ $^3A_2g \rightarrow {}^3T_1g(F)$	Octahedral
$[Co(L_1)_2Cl_2]\cdot 2H_2O$	4.19	35,714.28	32,258.06	20,833.33 15,873.01 13,888.88	$^4T_1g \rightarrow {}^4T_1g(P)$ $^4T_1g \rightarrow {}^4A_2g$ $^4T_1g \rightarrow {}^4T_2g(F)$	Octahedral
$[Cu(L_2)Cl\ (H_2O)_2].Cl$	1.61	37,037.03	33,333.33	13,333.33	$^2Eg \rightarrow {}^2T_2g$	Distorted Octahedral
$[Ni(L_2)Cl\ (H_2O)_2].Cl$	2.39	35,714.28	31,250.00	17,543.85 15,151.51	$^3A_2g \rightarrow {}^3T_1g(P)$ $^3A_2g \rightarrow {}^3T_1g(F)$	Octahedral
$[Co(L_2)Cl\ (H_2O)_2].Cl$	4.77	35,714.28	31,250.00	21,739.13 20,000.00 17,543.85	$^4T_1g \rightarrow {}^4T_1g(P)$ $^4T_1g \rightarrow {}^4A_2g$ $^4T_1g \rightarrow {}^4T_2g(F)$	Octahedral

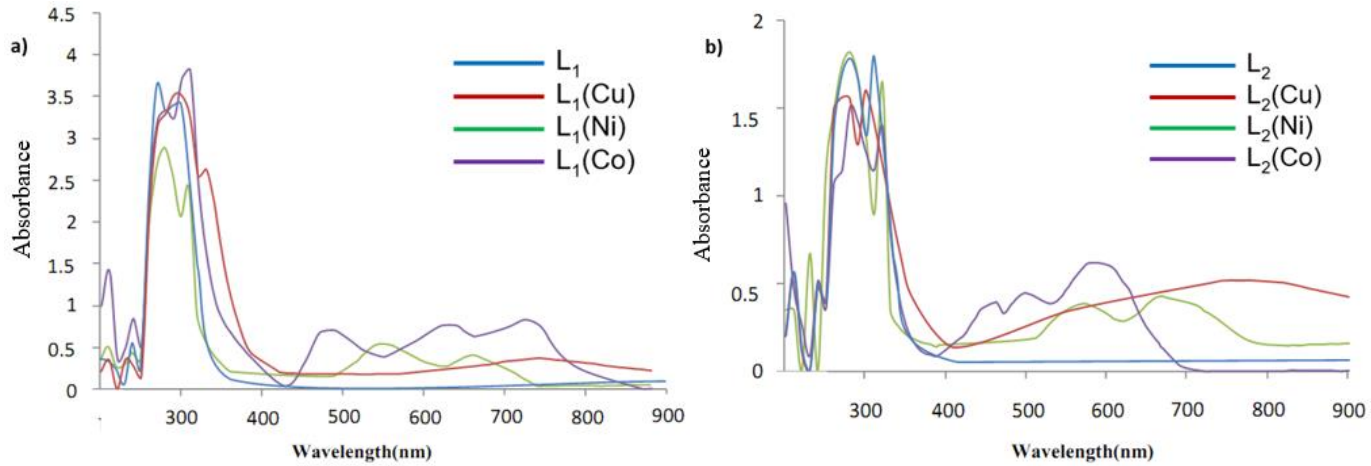

Figure 6. UV-Vis spectra. **(a) L₁** ligand and its complexes; **(b) L₂** ligand and its complexes.

3.4 Molar ratio (stoichiometry) of the studied complexes

Investigation of the molecular structure of the complexes formed between the metal ions of (Cu^{2+}, Ni^{2+}, and Co^{2+}) with ligands in **L₁** and **L₂** in methanol using molar ratio (Figs. 7 and 8) revealed the formation of (1:2) (M:L) complexes for **L₁** and (1:1) (M:L) complexes for **L₂** under investigation. The results are depicted in Table 4.

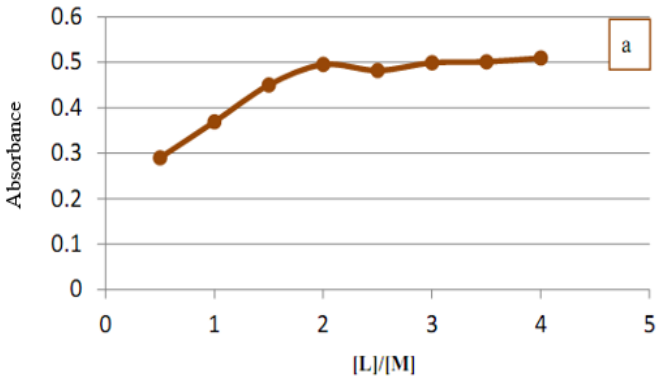

Eclética Química, vol. 48, n. 3, 2023, 36-53
ISSN: 1678-4618
DOI: 10.26850/1678-4618eqj.v48.3.2023.p36-53

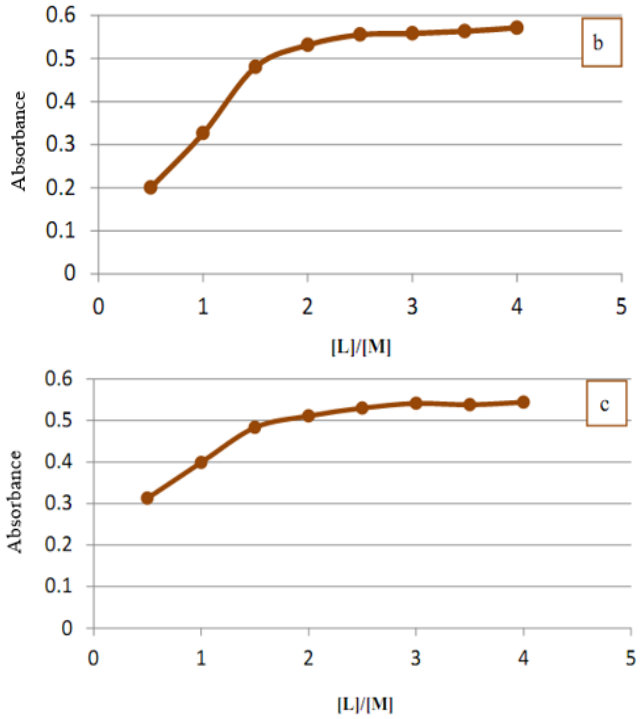

Figure 7. Molar ratio plot for the complexes between metal ions of **(a)** Cu, **(b)** Ni and **(c)** Co with $\mathbf{L_1}$ in methanol.

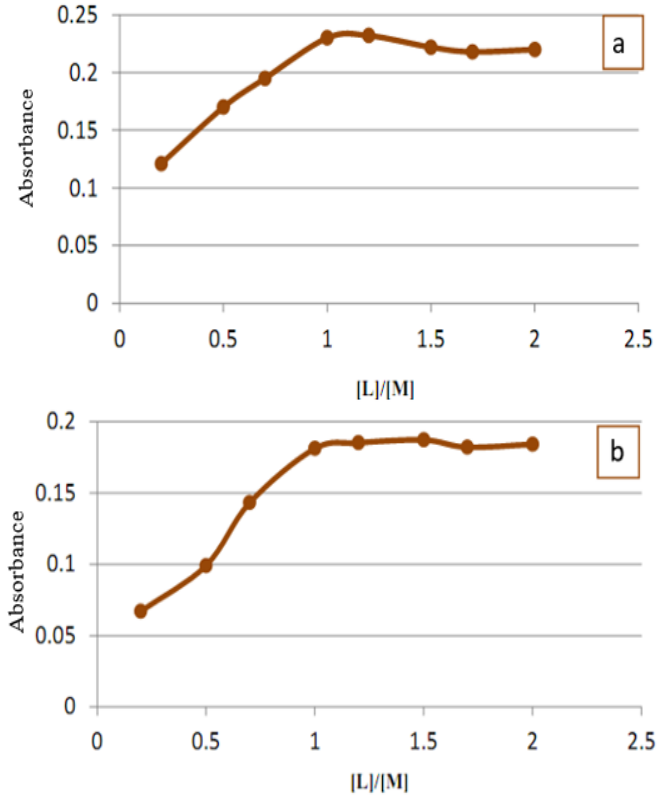

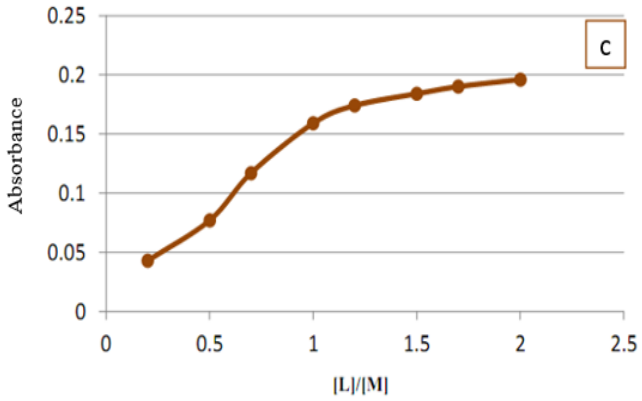

Figure 8. Molar ratio plot for the complexes between metal ions of **(a)** Cu, **(b)** Ni and **(c)** Co with $\mathbf{L_2}$ in methanol.

Table 4. Molar ratios for determination of stoichiometry of the $\mathbf{L_1}$ and $\mathbf{L_2}$complexes in methanol.

L_1			
[L]/[M]	**Absorbance of complexes**		
	Cu(II) λ = 330	Ni(II) λ = 310	Co(II) λ = 310
0.5:1	0.121	0.067	0.043
1:1	0.170	0.099	0.077
1.5:1	0.195	0.143	0.117
2:1	0.230	0.181	0.159
2.5:1	0.232	0.185	0.174
3:1	0.222	0.187	0.184
3.5:1	0.218	0.182	0.190
4:1	0.220	0.184	0.196
L_2			
[L]/[M]	**Absorbance of complexes**		
	Cu(II) λ = 300	Ni(II) λ = 320	Co(II) λ = 320
0.25:1	0.290	0.200	0.313
0.5:1	0.369	0.326	0.399
0.75:1	0.450	0.480	0.483
1:1	0.495	0.531	0.511
1.25:1	0.492	0.555	0.530
1.5:1	0.499	0.558	0.541
1.75:1	0.501	0.563	0.538
2:1	0.509	0.571	0.544

3.5 X-ray diffraction

The XRD patterns of the $\mathbf{L_1}$ and its complexes are shown in Fig. S5a–d (see Supplementary Material). The decrease of the XRD peak intensities of $\mathbf{L_1}$ complexes can be attributed to the reduction in crystallinities due to the complexation. This is in good agreement with the lowering in relative crystallinity calculated for these complexes (the crystallinity calculation in Table 5 is based on the integrated area of principal peaks of the complex to the $\mathbf{L_1}$ ligand obtaining a relative

Eclética Química, vol. 48, n. 3, 2023, 36-53
ISSN: 1678-4618
DOI: 10.26850/1678-4618eqj.v48.3.2023.p36-53

crystallinity) (Shah *et al*., 2006). The particle size calculated for **L₁** and its complexes (2.074–5.552 nm) in the range of nanoparticle size—the nanoparticle size reported in the literature ranges between 1–100 nm (Boverhof *et al*., 2015).

The particle size of **L₂** ligand was found within nanometric range (10.555 nm), nevertheless its complexes appeared as an amorphous character (Fig. S5e–h, see Supplementary Material). From this change, it is expected to improved properties of **L₂** complexes as compared with **L₂** ligand.

Table 5. Data of the principal values of intensity of the ligands and **L₁** complexes from XRD spectra.

Compound	2θ	β	D (nm)	Mean D	Xc (%)
L_1	6.780 13.720 18.880 19.960 23.920 28.220 29.900	0.340 0.419 0.459 0.405 0.379 0.295 0.337	4.266 3.480 3.154 3.630 3.905 5.061 4.447	3.991	100
L_2	12.799 16.740 25.441 31.040	0.120 0.153 0.121 0.180	12.142 9.464 12.268 8.349	10.555	100
$[Cu(L_1)_2Cl_2]\cdot 2H_2O$	6.719 13.460 18.599 20.919 31.659	0.352 0.562 0.229 0.237 0.178	4.120 2.576 6.407 6.213 8.455	5.552	10.392
$[Ni(L_1)_2Cl_2]\cdot 2H_2O$	16.279 32.761 33.579	0.439 0.240 0.232	3.332 6.033 6.241	5.202	18.506
$[Co(L_1)_2Cl_2]\cdot 2H_2O$	14.600 35.520 57.199 57.579	0.603 0.762 0.745 0.868	2.421 1.995 2.213 1.668	2.074	3.488

3.6 Antioxidant activity

The ligands and **L₂** complexes were investigated using FBRC technique to determine the antioxidant activity (Al-Azab *et al*., 2023).

Fe(II)-bipyridine complex produced by the reaction of Fe(III) with antioxidant followed by bipyridine exhibited maximum absorption at 535 nm (Fig. 9). Total antioxidant activity is based on the redox reaction between compounds and Fe(III) at room temperature. The initial antioxidant concentration is indicated by the concentration of the oxidizing Fe(III).

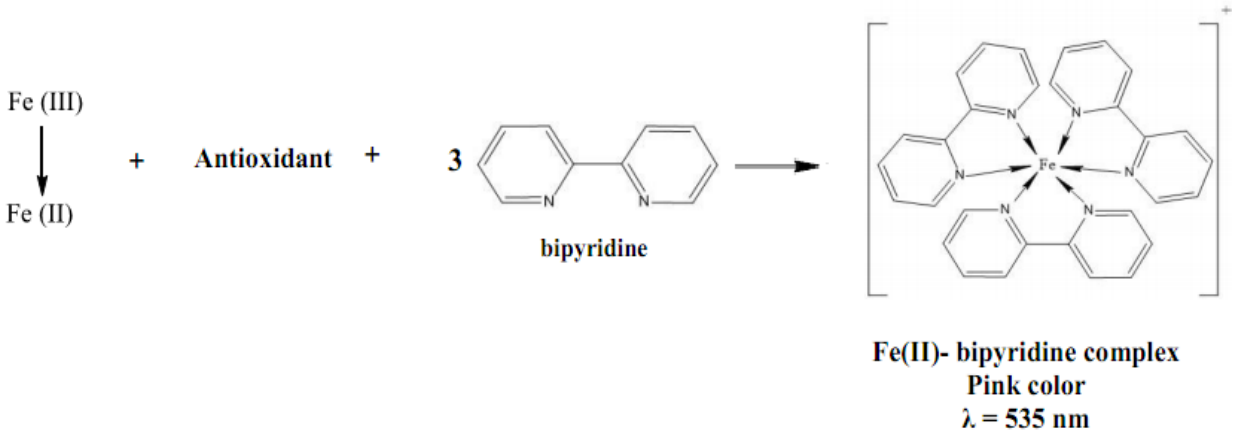

Figure 9. Stoichiometry outline of FBRC method.

Eclética Química, vol. 48, n. 3, 2023, 36-53
ISSN: 1678-4618
DOI: 10.26850/1678-4618eqj.v48.3.2023.p36-53

The results in Table 6 showed that these compounds were found to possess high potent antioxidant activity due presence of a combination of donor sites such as amide oxygen and imine nitrogen (Kostova and Saso, 2013).

Table 6. FBRC values express antioxidant activity as mg L^{-1} for prepared compounds to 1 mg L^{-1} of ascorbic acid

FBRC (mg L^{-1})	Sample
0.0248 ± 0.0001	**L_1**
0.0281 ± 0.0004	**L_2**
0.0201 ± 0.0002	$[Cu(L_2)Cl\ (H_2O)_2].Cl$
0.0183 ± 0.0002	$[Ni(L_2)Cl\ (H_2O)_2].Cl$ $[Ni(L_2)Cl{\cdot}(H_2O)_2].Cl$
0.0187 ± 0.0005	$[Co(L_2)Cl\ (H_2O)_2].Cl$ $[Co(L_2)Cl{\cdot}(H_2O)_2].Cl$

3.7 Antibacterial and antifungal screening for L_1, L_2 and their complexes

The synthetic ligands and their metal complexes havbeen examined for their antibacterial and antifungal activities using the disk diffusion method (Ericsson *et al.*, 1960) against four types of Bacteria (*Staphylococcus aureus, Bacillus subtilis, Escherichia coli, and Pseudomonas aeruginosa*) and one fungus (*Candida albicans*) on nutrient agar and Sabouraud dextrose agar (SDA) solid media, respectively. The inhibition zone diameter of the compounds is shown in Table 7 and Fig. 10a–d. From these results, it was noted that:

1- No inhibition zone was observed for ligands and their metal complexes against the fungus (*Candida albicans*);
2- The metal complexes are more potent bactericides than the ligands;
3- The order of antibacterial activity for the compounds with *Bacillus subtilis* was **L_1**(Cu) = **L_2**(Ni) > **L_1**(Ni) > **L_2**(Cu) > **L_2** > **L_1** > **L_1**(Co) = **L_2**(Co), with *Staphylococcus aureus* was **L_2**(Ni) > **L_1**(Cu) > **L_1**(Co) > **L_2**(Co) > **L_2** > **L_1** > **L_1**(Ni) = **L_2**(Cu), with *Escherichia Coli* was **L_1**(Co) > **L_1**(Cu) > **L_2**(Cu) > **L_2**(Co) > **L_2** > **L_1** > **L_1**(Ni) = **L_2**(Ni) and with *Pseudomonas aeruginosa* was **L_1**(Co) = **L_2**(Co) > **L_1**(Cu) > **L_2**(Ni) > **L_2** > **L_1** > **L_1**(Ni) = **L_2**(Cu).

In general, the complexes showed good antibacterial compared to the free ligands. Based on the chelation theory (Franklin and Snow, 1989), the increased inhibition activity of the metal complexes may be explained on the basis that their structures mainly possess C=N bonds. Besides, the coordination decreases the polarity of the metal ion due to the partial sharing of its positive charge with donor groups and possible π-electron delocalization inside the chelate ring-shaped during coordination that makes the complexes more lipophilic. This increased lipophilicity enhances the penetration of the metal complexes into lipid membranes, blocks the metal binding sites in the enzymes, and limits the further development of the organisms.

Table 7. Biological activities of the ligands and their metal complexes against bacteria and fungus (zone of inhibition in mm).

Compound (1000/mL^{-1})	Bacteria				Fungi
	gram-positive		gram-negative		
	Bacillus subtilis	*Staphylococcus aureus*	*Escherichia coli*	*Pseudomonas aeruginosa*	*Candida albicans*
L_1	5	3	4	3	0
L_2	6	5	6	5	0
$[Cu(L_1)_2Cl_2].2H_2O$	11	8	9	10	0
$[Ni(L_1)_2Cl_2].2H_2O$	10	0	0	0	0
$[Co(L_1)_2Cl_2].2H_2O$	0	7	10	15	0
$[Cu(L_2)Cl\ (H_2O)_2].Cl$ $[Cu(L_2)Cl{\cdot}(H_2O)_2].Cl$	7	0	8	0	0
$[Ni(L_2)Cl\ (H_2O)_2].Cl$ $[Ni(L_2)Cl{\cdot}(H_2O)_2].Cl$	11	10	0	7	0
$[Co(L_2)Cl\ (H_2O)_2].Cl$ $[Co(L_2)Cl{\cdot}(H_2O)_2].Cl$	0	6	7	15	0
Gentamicin (120 µg/ml)	29	25	23	28	-
Mycostatin (30 µg/ml)	-	-	-	-	18

Eclética Química, vol. 48, n. 3, 2023, 36-53
ISSN: 1678-4618
DOI: 10.26850/1678-4618eqj.v48.3.2023.p36-53

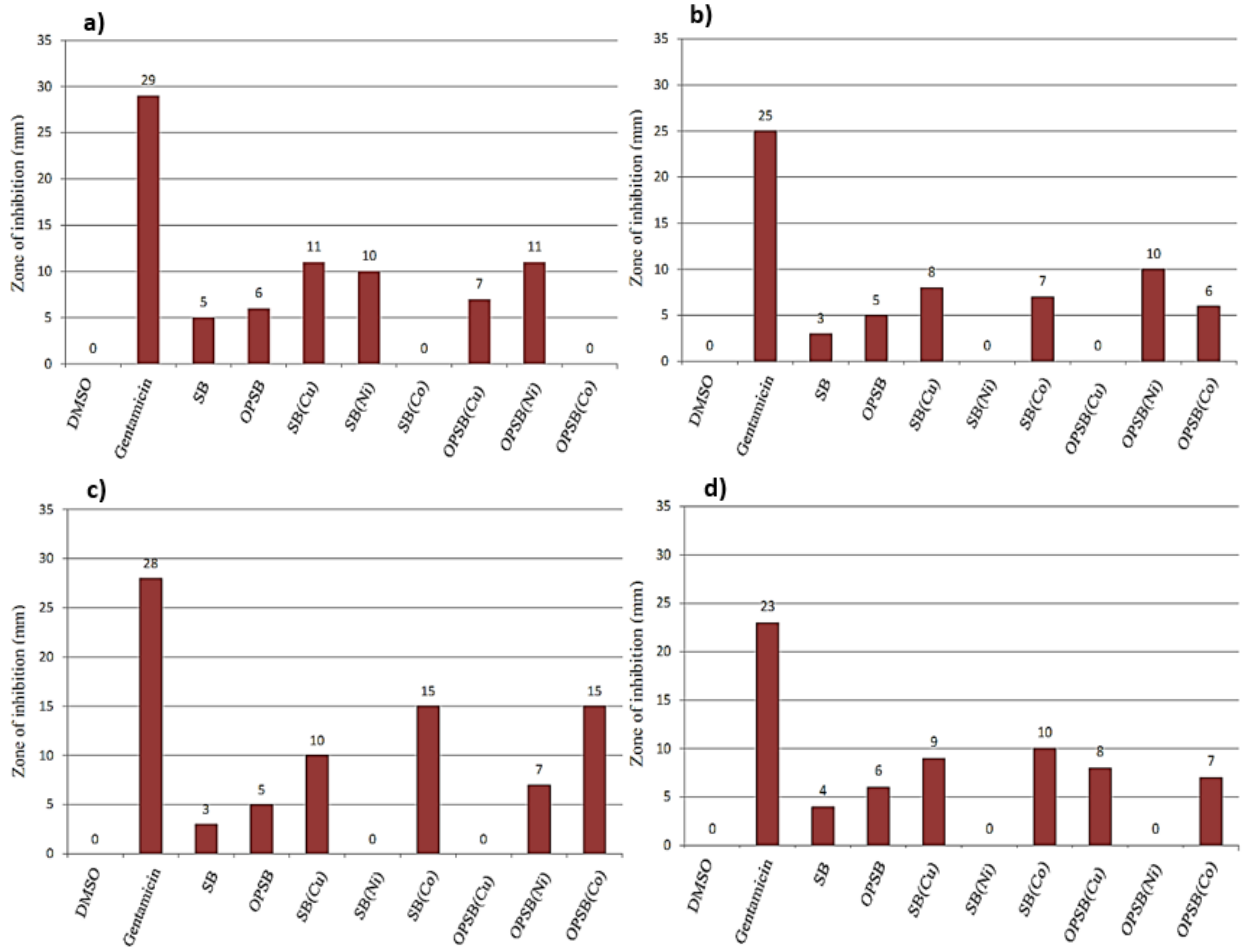

Figure 10. Antibacterial activity of the ligands and their metal complexes against gram-positive bacterium **(a)** *Bacillus subtilis*; **(b)** *Staphylococcus aureus*; **(c)** *Pseudomonas aeruginosa*; and gram-negative bacterium **(d)** *Escherichia coli*.

4. Conclusions

In summary, the synthesis and physicochemical analysis were done for new ligands $\mathbf{L_1}$ and $\mathbf{L_2}$ with their complexes. In complexes, the ligand $\mathbf{L_1}$ acts as neutral-bidentate and $\mathbf{L_2}$ acts as neutral-tridentate around the metallic ion. Electronic properties and magnetic susceptibility suggested octahedral geometry for all complexes. According to XRD, the ligands and $\mathbf{L_1}$ complexes were in the nanoscale (2.074–10.555 nm). The ligands and $\mathbf{L_2}$ complexes gave high antioxidant activity using FBRC technique. All compounds have been screened for their antibacterial and antifungal activity.

Authors' contribution

Conceptualization: Jamil, Y. M.; Al-Azab, F. M.
Data curation: Al-Selwi, N. A.
Formal Analysis: Jamil, Y. M.; Al-Selwi, N. A.
Funding acquisition: Not applicable.
Investigation: Jamil, Y. M.; Al-Azab, F. M.; Al-Selwi, N. A.
Methodology: Jamil, Y. M.; Al-Azab, F. M.; Al-Selwi, N. A.
Project administration: Jamil, Y. M.; Al-Azab, F. M.
Resources: Jamil, Y. M.; Al-Azab, F. M.; Al-Selwi, N. A.
Software: Al-Selwi N. A.
Supervision: Jamil, Y. M.; Al-Azab, F. M.
Validation: Jamil, Y. M.; Al-Azab, F. M.
Visualization: Jamil, Y. M.; Al-Azab, F. M.; Al-Selwi, N. A.
Writing – original draft: Al-Selwi, N. A.
Writing – review & editing: Jamil, Y. M.

Eclética Química, vol. 48, n. 3, 2023, 36-53
ISSN: 1678-4618
DOI: 10.26850/1678-4618eqj.v48.3.2023.p36-53

Data availability statement

All data sets were generated or analyzed in the current study

Funding

Not applicable.

Acknowledgments

Not applicable.

References

Abd El-Wahab, Z. H.; El-Sarrag, M. R. Derivatives of phosphate Schiff base transition metal complexes: synthesis, studies and biological activity. *Spectrochimica Acta Part A.* **2004**, *60*, 271–277. https://doi.org/10.1016/S1386-1425(03)00216-6

Abu-Dief, A. M.; El-Metwaly, N. M.; Alzahrani, S. O.; Bawazeer, A. M.; Shaaban S.; Adam, M. S. S. Targeting *ct*DNA binding and elaborated in-vitro assessments concerning novel Schiff base complexes: Synthesis, characterization, DFT and detailed in-silico confirmation. *J. Mol. Liq.* **2021**, *322*, 114977. https://doi.org/10.1016/j.molliq.2020.114977

Abu-Yamin, A.; Abduh, M. S.; Saghir, S. A. M.; Al-Gabri, N. Synthesis, characterization and biological activities of new Schiff base compound and its lanthanide complexes. *Pharmaceuticals* **2022**, *15* (4), 454. https://doi.org/10.3390/ph15040454

Aderoju, A. O.; Sherifah, M. W. Synthesis, characterization and antimicrobial activity of some mixed drug trimethoprim-sulfamethoxazole metal drug complexes. *World Appl. Sci. J.* **2015**, *33* (2), 336–342. https://doi.org/10.5829/idosi.wasj.2015.33.02.22206

Akhtar M. S.; Alenad, A.; Malik, M. A. Synthesis of mackinawite FeS thin films from acidic chemical baths. *Mater. Sci. Semicond. Process.* **2015**, *32*, 1–5. https://doi.org/10.1016/j.mssp.2014.12.073

Al-Azab, F. M.; Jamil, Y. M. S.; Al-Gaadbi,A. A. M., Synthesis and Spectroscopic methods on the Complexation of CoII, NiII and CuII with 2-(((1H-indol-3-yl) methylene) amino) acetohydrazide hydrate. Sana'a University J. Appl. Sci. Technol. **2023**, *1* (1), 117–133. https://doi.org/10.59628/jast.v1i1.131

Al-Hakimi, A. N.; Shakdofa, M. M. E.; El-Seidy, A. M. A.; El-Tabl, A. S. Synthesis, Spectroscopic, and biological studies of chromium(iii), manganese(ii), iron(iii), cobalt(ii), nickel(ii), copper(ii), ruthenium(iii), and zirconyl(ii) complexes of N1,N2-Bis(3-((3-hydroxynaphthalen-2-yl)methylene-amino)propyl)phthalamide. *J. Korean Chem. Soc.* **2011**, *55* (3), 418–429. https://doi.org/10.5012/jkcs.2011.55.3.418

Al-Maydama, H.; Al-Ansi, T. Y.; Jamil, Y. M.; Ali, A. H. Biheterocyclic ligands: synthesis, characterization and coordinating properties of bis(4-amino-5-mercapto-1,2,4-triazol-3-yl)alkanes with transition metal ions and their thermokinetic and biological studies. *Eclét. Quím.* **2008**, *33* (3), 29–42. https://doi.org/10.1590/S0100-46702008000300005

Boverhof, D. R.; Bramante, C. M.; Butala, J. H.; Clancy, S. F.; Lafranconi, M.; West, J.; Gordon, S. C. Comparative assessment of nanomaterial definitions and safety evaluation considerations. *Regul. Toxicol. Pharmacol.* **2015**, *73* (1), 137–150. https://doi.org/10.1016/j.yrtph.2015.06.001

Brzezińska-Błaszczyk, E.; Mińcikiewicz, M.; Ochocki, J. Effect of cisplatin and *cis*-platinum (II) phosphonate complex on murine mast cells. *Eur. J. Pharmacol*. **1996**, *298* (2), 155–158. https://doi.org/10.1016/0014-2999(95)00809-8

Çakır, U.; Temel, H.; Ihan, S.; Uğraş, H. I. Spectroscopic and conductance studies of new transition metal complexes with a Schiff base derived from 4-methoxybenzaldehyde and 1,2-bis(*p*-aminophenoxy)ethane. *Spectrosc. Lett.* **2003**, *36* (5–6), 429–440. https://doi.org/10.1081/SL-120026609

Camellia, F. K.; Ashrafuzzaman, M.; Islam, M. N.; Banu, L. A.; Kudrat-E-Zahan, M. Isoniazid Derived Schiff Base Metal Complexes: Synthesis, Characterization, Thermal Stability, Antibacterial and Antioxidant Activity Study. *Asian J. Chem. Sci.* **2022**, *11* (4), 23-36. https://doi.org/10.9734/ajocs/2022/v11i419131

Carrasco, F.; Hernández, W.; Chupayo, O.; Álvarez, C. M.; Oramas-Royo, S.; Spodine, E.; Tamariz-Angeles, C.; Olivera-Gonzales, P.; Dávalos, J. Z. Indole-3-carbaldehyde semicarbazone derivatives: Synthesis, characterization and antibacterial activities. *J. Chem.* **2020**, *2020*, 7157281. https://doi.org/10.1155/2020/7157281

Ceramella, J.; Iacopetta, D.; Catalano, A.; Cirillo, F.; Lappano, R.; Sinicropi, M. S. A Review on the antimicrobial activity of Schiff bases: data collection and recent studies. *Antibiotics* **2022**, *11* (2), 191. https://doi.org/10.3390/antibiotics11020191

El-khazandar, A. N. Organo-phosphorus Schiff base part (IV): Synthesis and characteristic of some phosphate Schiff-base complexes. *Phosphorus Sulfur Silicon Relat. Elem.* **1997**, *126* (1), 243–255. https://doi.org/10.1080/10426509708043564

El-Tabl, A. S.; El-Saied, F. A.; Al-Hakimi, A. N. Synthesis, spectroscopic investigation and biological activity of metal complexes with ONO trifunctionalalized hydrazone ligand. *Transition Met. Chem.* **2007**, *32* (6), 689–701. https://doi.org/10.1007/s11243-007-0228-0

Ericsson, H.; Tunevall, G.; Wickman, K. The Paper Disc Method for Determination of Bacterial Sensitivity to Antibiotics: Relationship Between the Diameter of the Zone

Eclética Química, vol. 48, n. 3, 2023, 36-53
ISSN: 1678-4618
DOI: 10.26850/1678-4618eqj.v48.3.2023.p36-53

of Inhibition and the Minimum Inhibitory Concentration. *Scand. J. Clin. Lab. Invest.* **1960**, *12* (4), 414–422. https://doi.org/10.3109/00365516009065406

Fouda, M. F. R.; Abd-Elzaher, M. M.; Shakdofa, M. M.; El-Saied, F. A.; Ayad, M. I.; El Tabl, A. S. Synthesis and characterization of a hydrazone ligand containing antipyrine and its transition metal complexes. *J. Coord. Chem*. **2008**, *61* (12), 1983–1996. https://doi.org/10.1080/00958970701795714

Franklin, T. J.; Snow, G. A. *Biochemistry of Antimicrobial Action*; Springer, 1989. https://doi.org/10.1007/978-94-009-0825-3

Galil, M. S. A.; Al-Hakimi, A. N.; Alshwafy, R. Y.; Al Okab, R. A.; Mutir, A. Synthesis, Structural Studies and Microbial Evaluation of Cu(II), Mn(II) Ni(II), Zn(II), Fe(III), Ru(III), VO(II), UO_2(II) Complexes of Tetradentate Oxime-Hydrazon Ligand. *Chem. J.* **2015**, *1* (3), 95–102.

Geary, W. J. The use of conductivity measurements in organic solvents for characterization of coordination compounds. *Coord. Chem. Rev.* **1971**, *7* (1), 81–122. https://doi.org/10.1016/S0010-8545(00)80009-0

González-García, C.; Mata, A.; Zani, F.; Mendiola M. A.; López-Torres, E. Synthesis and antimicrobial activity of tetradentate ligands bearing hydrazone and/or thiosemicarbazone motifs and their diorganotin (IV) complexes. *J. Inorg. Biochem.* **2016**, *163*, 118–130. https://doi.org/10.1016/j.jinorgbio.2016.07.002

Gup, R.; Kirkan, B. Synthesis and spectroscopic studies of copper(II) and nickel(II) complexes containing hydrazonic ligands and heterocyclic colig and Spectrochim. *Acta Part A Mol. Biomol. Spectrosc*. **2005**, *62* (4–5), 1188–1195. https://doi.org/10.1016/j.saa.2005.04.015

Hossain, M. S.; Camellia, F. K.; Uddin, N.; Kudrat-E-Zahan, M.; Banu, L. A.; Haque, M. M. Synthesis, Characterization and Antimicrobial Activity of Metal Complexes of N-(4-methoxybenzylidene) Isonicotinohydrazone Schiff Base. *Asian J. Chem. Sci.* **2019**, *6* (1), 1–8. https://doi.org/10.9734/ajocs/2019/v6i118987

Ibeji, C. U.; Akintayo, D. C.; Oluwasola, H. O.; Akintemi, E. O. Anti-Corrosion potential of the Ortho and ParaSubstituted Schiff Bases of 2-Methoxybenzaldehyde on Fe (110) surface in acid medium: Synthesis, DFT and Molecular Dynamics Studies. *Research square.* **2022**. [Preprint]. https://doi.org/10.21203/rs.3.rs-1869552/v1

Jamil, Y.M.S.; Al-Azab, A. M.; Al-Azab, F. M.; Al-Selwi, N. A. A. Larvicidal Effects of New Organophosphorus Schiff base compounds against Dengue Fever Vector *Aedes aegypti* (Diptera; Culicidae), *Sana'a University J. Appl. Sci. Technol.* **2023**, *1* (1), 78–87. https://doi.org/10.59628/jast.v1i1.156

Jassem, A. M.; Radhi, W. A.; Jaber, H. A.; Mohammed, F. J. Synthesis and characterization of 1,3,4-Oxadiazoles Derivatives from 4-Phenyl-Semicarbazide. *J. Basrah Res. Sci.* **2013**, *39* (3), 158–170.

Kaczmarek, M. T.; Zabiszak, M.; Nowak, M.; Jastrzab, R. Lanthanides: Schiff base complexes, applications in cancer diagnosis, therapy, and antibacterial activity. *Coord. Chem. Rev.* **2018**, *370*, 42–54. https://doi.org/10.1016/j.ccr.2018.05.012

Kafi-Ahmadi, L.; Marjani, A. P. Mononuclear Schiff Base Complexes Derived from 5-Azophenylsalicylaldehyde with Co(II), Ni(II) Ions: Synthesis, Characterization, Electrochemical Study and Antibacterial Properties. *S. Afr. J. Chem.* **2019**, *72* (1), 101–107. https://doi.org/10.17159/0379-4350/2019/v72a13

Kostova, I.; Saso, L. Advances in Research of Schiff-Base Metal Complexes as Potent Antioxidants. *Curr. Med. Chem.* **2013**, *20* (36), 4609–4632. https://doi.org/10.2174/09298673113209990149

Mohammed, N. L.; Al-Shawi, J. M. S.; Kadhim, M. J. Synthesis, Characterization and Thermal Studies of Schiff Bases Derived from 2,4-Dihydroxy benzaldehyde and their Complexes with Co(II), Ni (II), Cu(II). *Int. J. Sci. Eng. Res.* **2019**, *7* (1), 31–40.

Mohapatra, R. K.; Mishra, U. K.; Mishra, S. K.; Mahapatra, A.; Dash, D. C. Synthesis and Characterization of Transition Metal Complexes with Benzimidazolyl-2-hydrazones of o-anisaldehyde and Furfural. *J. Korean Chem. Soc.* **2011**, *55* (6), 926–931. https://doi.org/10.5012/jkcs.2011.55.6.926

Nakamoto, K. *Infrared and Raman Spectra of Inorganic and Coordination Compounds*. Part A and Part B; John Wiley & Sons, 1998.

Ochocki, J.; Graczyk, J.; Reedijk, J. Synthesis and antitumor activity of novel Pt(II) diethyl pyridylmethylphosphonate complexes against sarcoma-180. *J. Inorg. Biochem.* **1995**, *59* (2–3), 240. https://doi.org/10.1016/0162-0134(95)97346-R

Patterson, A. L. The Scherrer Formula for X-Ray Particle Size Determination. *Phys. Rev.* **1939**, *56* (10), 978–982. https://doi.org/10.1103/PhysRev.56.978

Sani, U.; Iliyasu, S. M. Synthesis, characterization and antimicrobial studies on Schiff base derived from 2-aminopyridine and 2-methoxybenzaldehyde and its cobalt (II) and nickel (II) complexes. *Bayero J. Pure appl. Sci.* **2018**, *11* (1), 214–219. https://doi.org/10.4314/bajopas.v11i1.35S

Shah, B.; Kakumanu, V. K.; Bansal, A. K. Analytical techniques for quantification of amorphous/crystalline phases in pharmaceutical solids. *J. Pharm. Sci.* **2006**, *95* (8), 1641–1665. https://doi.org/10.1002/jps.20644

Shakdofa, M. M. E.; Al-Hakimi, A. N.; Elsaied, F. A.; Alasbahi, S. O. M.; Alkwlini, A. M. A. Synthesis, Characterization and Bioactivity Zn^{2+}, Cu^{2+}, Ni^{2+}, Co^{2+}, Mn^{2+}, Fe^{3+}, Ru^{3+}, VO^{2+} and UO^{2+} complexes of 2-hydroxy-5-((4-

Eclética Química, vol. 48, n. 3, 2023, 36-53
ISSN: 1678-4618
DOI: 10.26850/1678-4618eqj.v48.3.2023.p36-53

nitrophnyl(dizenyl)benzylidene)-2-(p-tolylamino)acetohydrazide. *Bull. Chem. Soc. Ethiop*. **2017**, *31* (1), 75–91. https://doi.org/10.4314/bcse.v31i1.7

Song, X.-Q.; Wang, Z.-G.; Wang, Y.; Huang, Y.-Y.; Sun, Y.-X.; Ouyang, Y.; Xie, C.-Z.; Xu, J.-Y. Syntheses, characterization, DNA/HSA binding ability and antitumor activities of a family of isostructural binuclear lanthanide complexes containing hydrazine Schiff base. *J. Biomol. Struct. Dyn.* **2020**, *38* (3), 733–743. https://doi.org/10.1080/07391102.2019.1587511

Vogel, A. I. *Text-book of quantitative inorganic analysis including elementary instrumental analysis*; Longmans, 1961.

Yassin, S. K.; Alshawi J. M. S.; Salih, Z. A. M. Synthesis, characterization and cytotoxic activity study of Cu (II), Co (II), Mn (II), Ni (II) and Cr (III) Metal Complexes with new guanidine Schiff base against the hepatocellular Carcinoma (HCAM) cancer cell. *Egypt. J. Chem.* **2020**, *63* (10), 4005-4016. https://doi.org/10.21608/ejchem.2020.37893.2778

Yoe, J. H.; Jones, A. L. Colorimetric Determination of Iron with Disodium-1,2-dihydroxybenzene-3,5-disulfonate. *Ind. Eng. Chem. Anal. Ed*. **1944**, *16* (2), 111–115. https://doi.org/10.1021/i560126a015

Yusof, E. N. M.; Ravoof, T. B. S. A.; Tiekink, E. R. T.; Veerakumarasivam, A.; Crouse, K. A.; Tahir, M. I. M.; Ahmad, H. Synthesis, Characterization and Biological Evaluation of Transition Metal Complexes Derived from N, S Bidentate Ligands. *Int. J. Mol. Sci.* **2015**, *16* (5), 11034–11054. https://doi.org/10.3390/ijms160511034

Eclética Química, vol. 48, n. 3, 2023, 36-53
ISSN: 1678-4618
DOI: 10.26850/1678-4618eqj.v48.3.2023.p36-53

Supplementary Materials

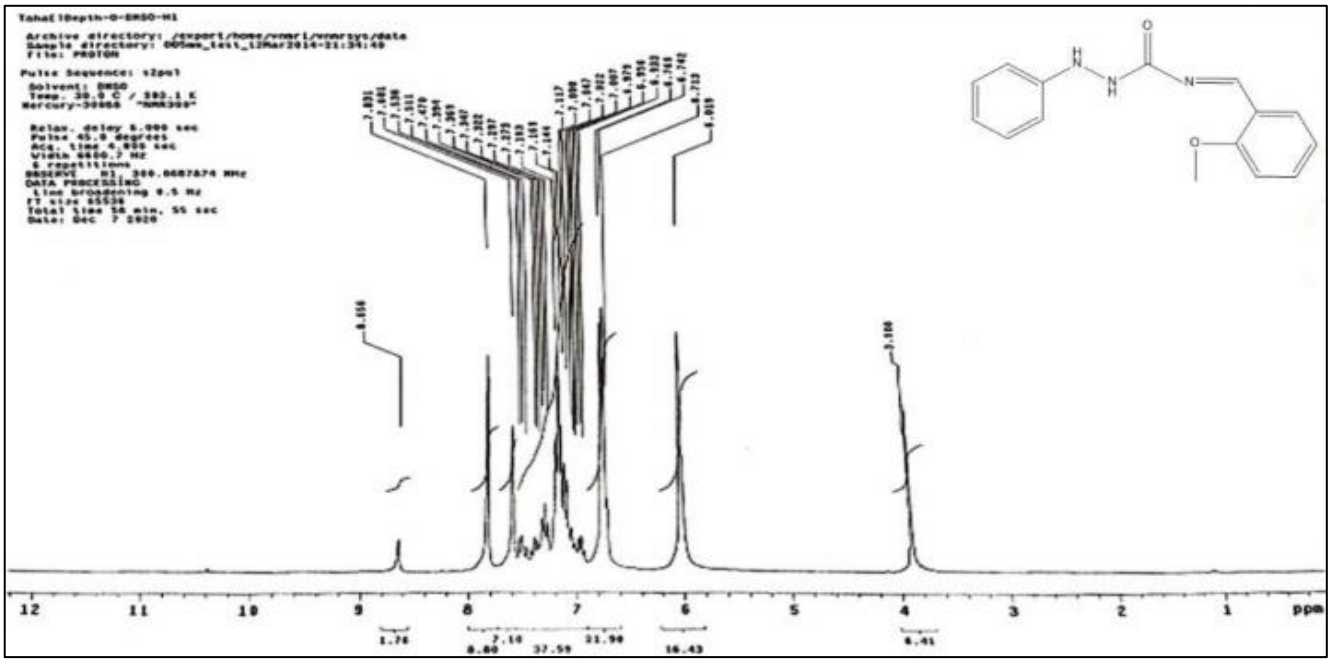

Figure S1. [1]HNMR spectrum of $\mathbf{L_1}$.

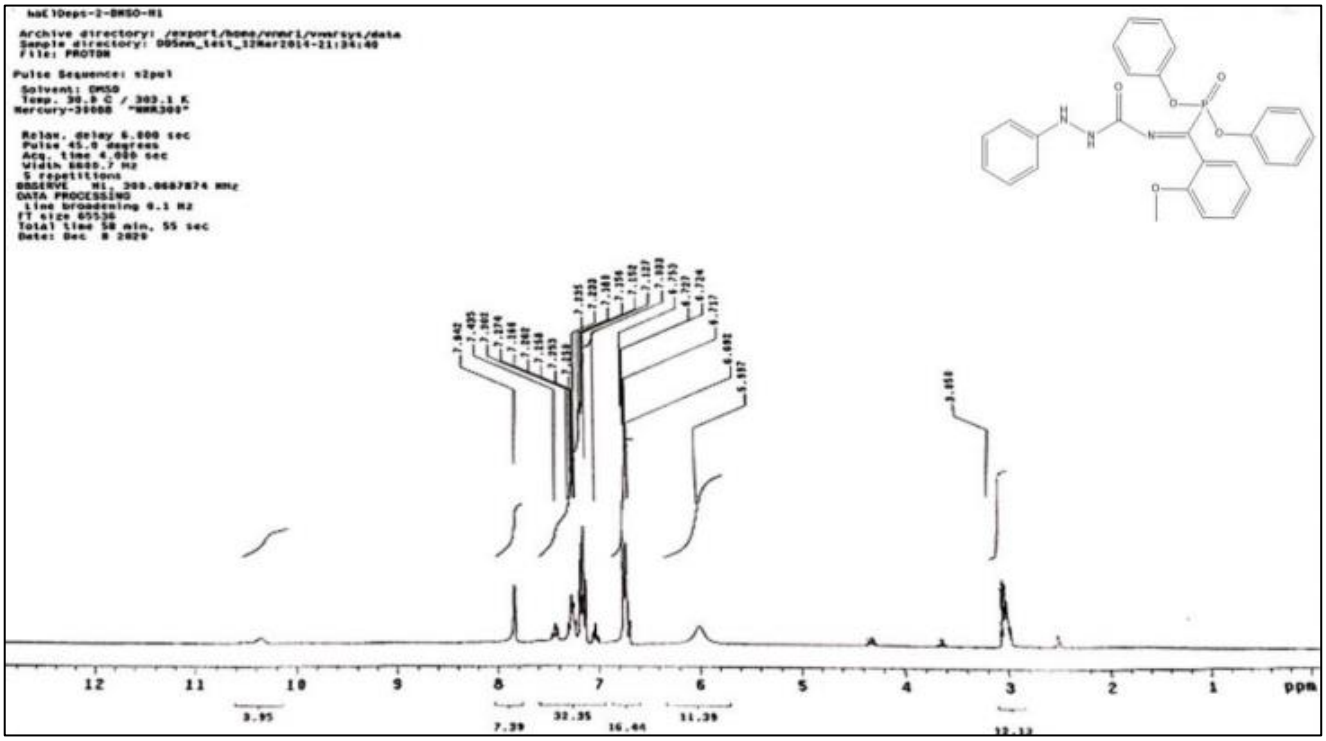

Figure S2. [1]HNMR spectrum of $\mathbf{L_2}$.

Eclética Química, vol. 48, n. 3, 2023, 36-53
ISSN: 1678-4618
DOI: 10.26850/1678-4618eqj.v48.3.2023.p36-53

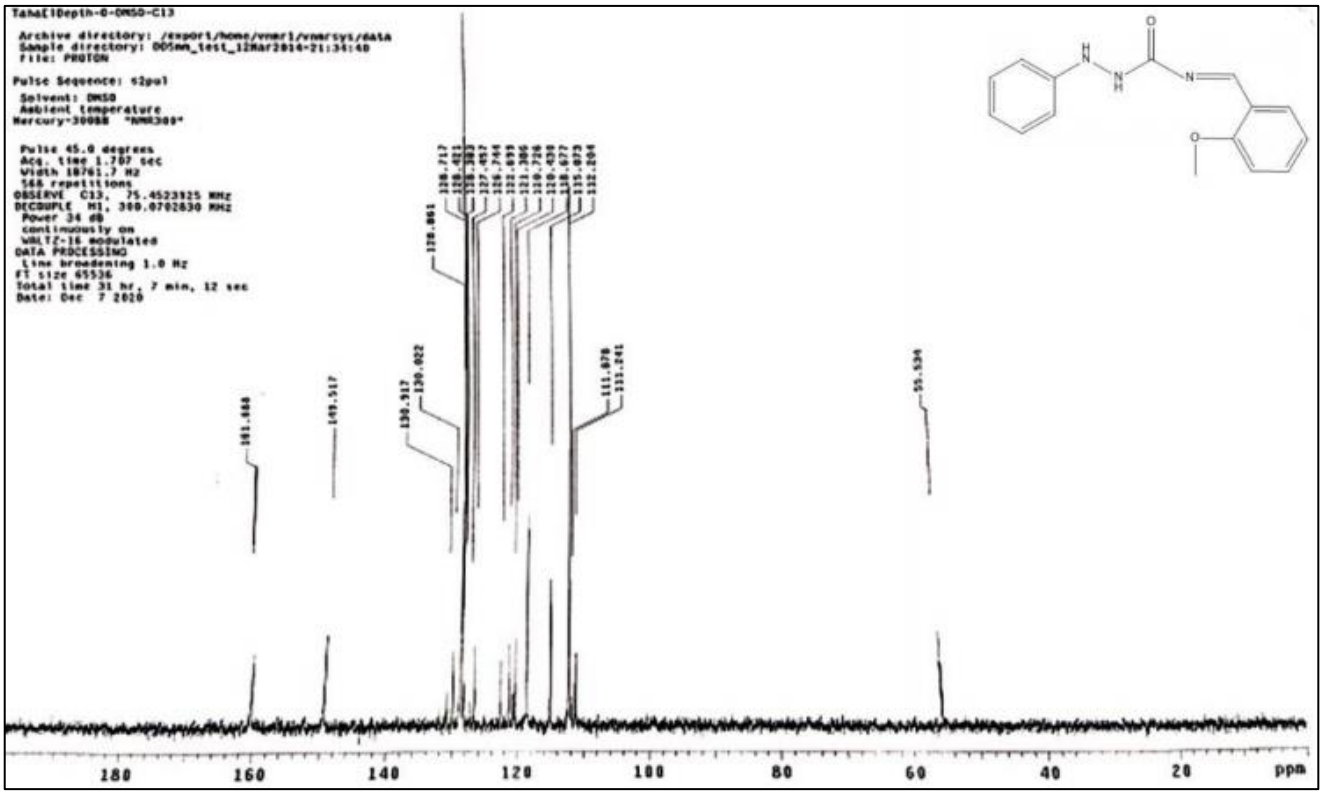

Figure S3. ^{13}CNMR spectrum of **L_1**.

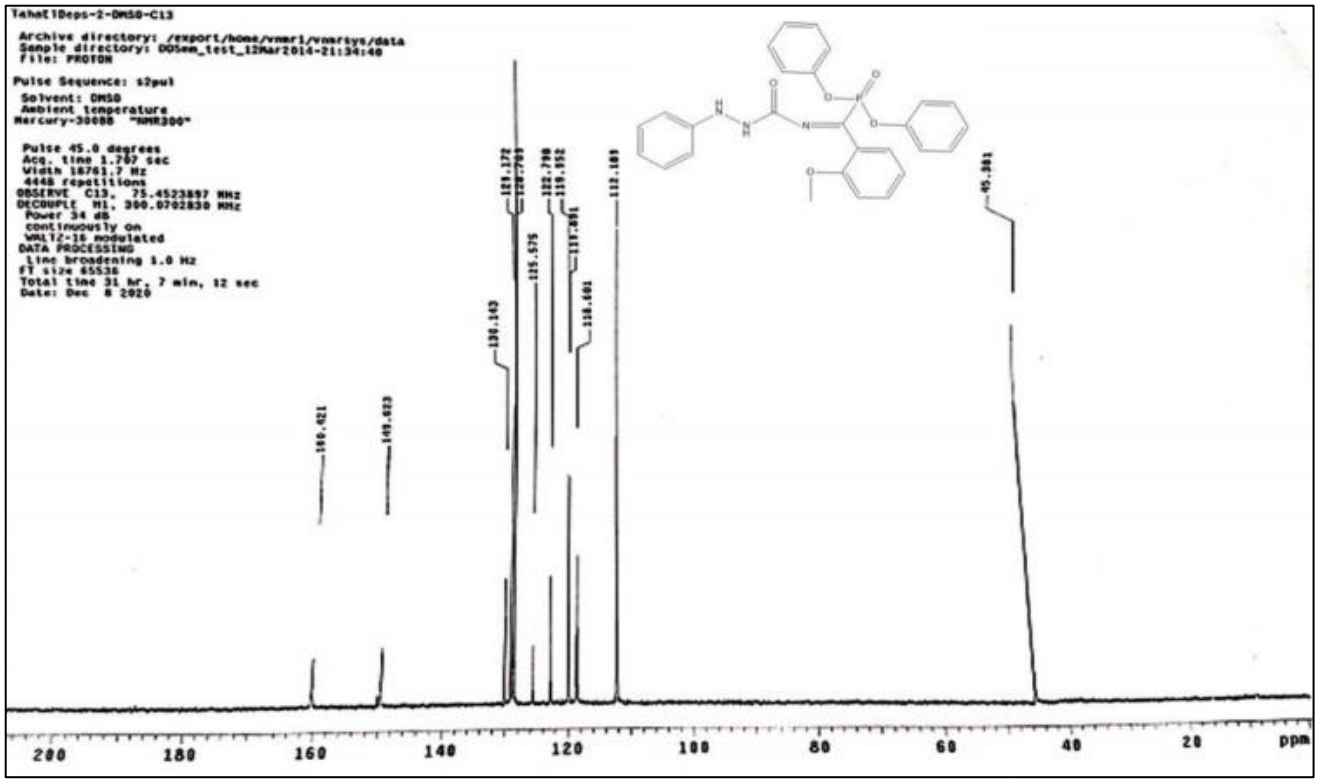

Figure S4. ^{13}CNMR spectrum of **L_2**.

Eclética Química, vol. 48, n. 3, 2023, 36-53
ISSN: 1678-4618
DOI: 10.26850/1678-4618eqj.v48.3.2023.p36-53

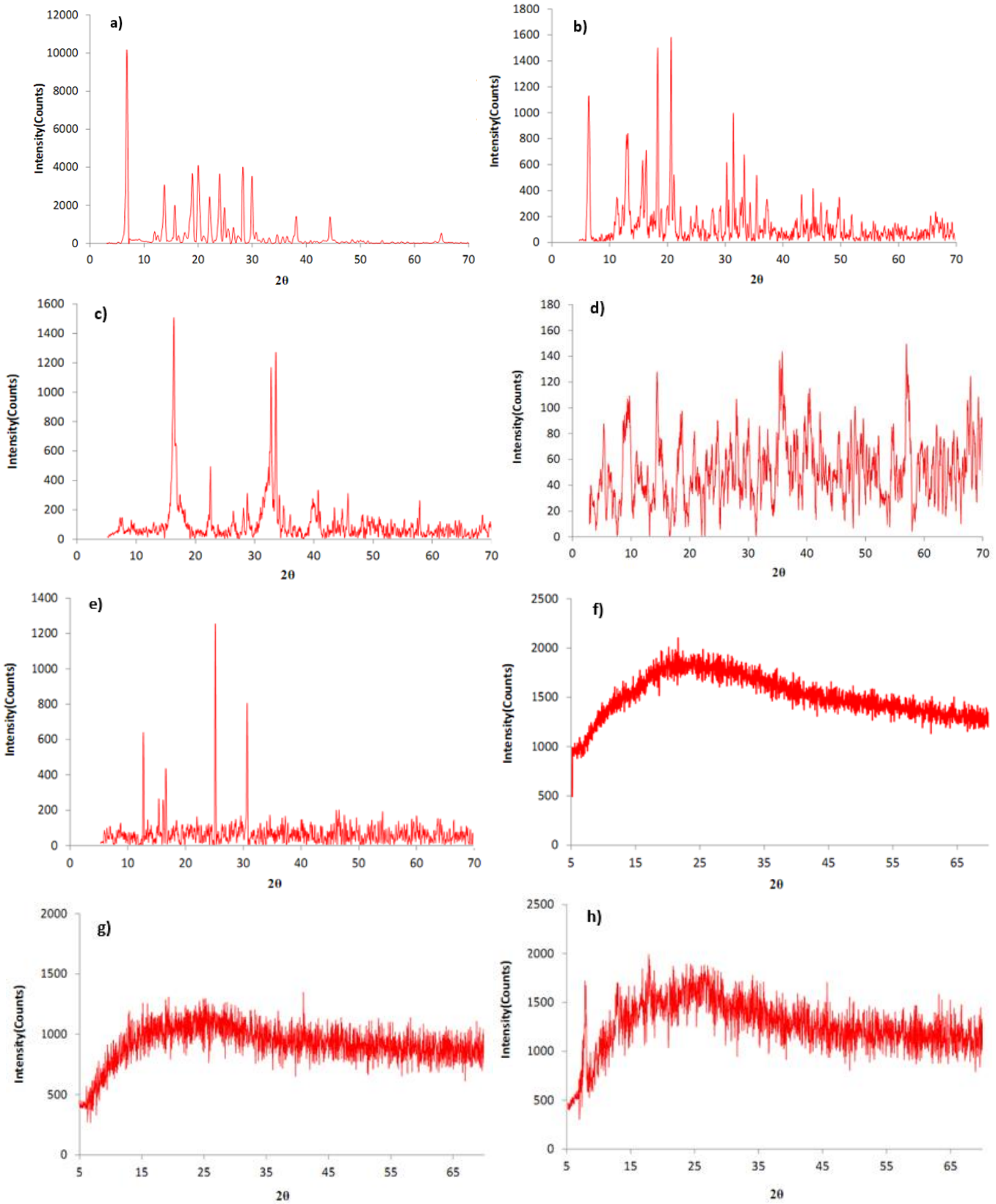

Figure S5. XRD pattern of **(a)** L_1; **(b)** L_1(Cu); **(c)** L_1(Ni); **(d)** L_1(Co); **(e)** L_2; **(f)** L_2(Cu); **(g)** L_2(Ni); **(h)** L_2(Co);

Eclética Química, vol. 48, n. 3, 2023, 36-53
ISSN: 1678-4618
DOI: 10.26850/1678-4618eqj.v48.3.2023.p36-53